Applied Radiation and Isotopes 168 (2021) 109518

Contents lists available at ScienceDirect

Applied Radiation and Isotopes

journal homepage: http://www.elsevier.com/locate/apradiso

X-ray-based positioning method for mars entry blackout mitigation

Peng Dang [a], Xiaobin Tang [a,b,*], Yunpeng Liu [a,b], Junxu Mu [a], Sheng Lai [a]

[a] Department of Nuclear Science and Technology, Nanjing University of Aeronautics and Astronautics, Nanjing, 210016, China
[b] Key Laboratory of Nuclear Technology Application and Radiation Protection in Astronautics, Ministry of Industry and Information Technology, Nanjing, 210016, China

ARTICLE INFO

Keywords:
X-ray signal
Mars entry blackout
Positioning method
Plasma sheath
Martian atmosphere

ABSTRACT

Enhancing the positional information acquisition during Mars entry blackout improves the Mars landing mission reliability. A positioning method based on the high-penetration of X-rays was developed to solve the problem. The X-ray signal attenuation was estimated. The positioning performance and the influence of X-ray signal transmission system were also evaluated. Results indicated that the X-ray signal attenuation is extremely low, and the X-ray-based method is expected to be a potential application for obtaining high-precision positional information during Mars entry blackout.

1. Introduction

X-rays have been used in many technology fields since their discovery in 1895. In some space technologies, X-rays also present superiorities (Economou, 2010). Due to the strong penetrability, X-rays in the plasma sheath of the spacecraft communication blackout nearly have no attenuation (Li et al., 2017; Li et al., 2020). When the spacecraft enters into the planetary atmosphere from outer space, a plasma sheath generated by high-speed flight is commonly formed on the entry vehicle surface and disrupts the signal transmission (Kim and Gülhan, 2011; Ramjatan et al., 2017). Mars entry vehicles also experience the process, which is called Mars entry blackout (Lévesque and De Lafontaine, 2007; Wang and Xia, 2015). Future Mars missions, such as sample return and manned landing, demand the capability of pinpoint landing at a predefined site (Drake et al., 2010; Salotti and Heidmann, 2014). However, most of the sensors cannot be worked under the harsh conditions of Mars entry blackout (Li and Jiang, 2014). Based on the high penetration, X-ray signals are expected to enhance the acquisition of positional information for future Mars landing missions.

The position estimation of all probes which have been successfully landed on Mars is realized primarily with the inertial measurement unit (IMU) based dead reckoning method (Jah et al., 2008; Yu et al., 2017). Nevertheless, previous studies have shown that the positioning error of IMU, even if corrected through other means before the Mars entry blackout occurred, while still exceeds a few hundred meters (Li and Peng, 2011). This increases the failure risk of future Mars pinpoint landing missions. Moreover, the concept, such as Mars Network, which utilizing the transceiver carried by the entry vehicle to receive the radio frequency (RF) signals from beacons or orbiters has been proposed for achieving the increased accuracy in the landing process (Hastrup et al., 2003; Lightsey et al., 2008). Although this concept is capable to reduce the positioning error, the disruption of RF signals during Mars entry blackout still is a critical issue that needs to be resolved.

The aim of this work is to introduce a positioning method which establishes the X-ray signal transmission link between the entry vehicle and orbiters for obtaining the positional information during Mars entry blackout. This paper is structured as followed: Section 2 describes the design and realization of this scheme and introduces the measurement model and X-ray signal transmission link model. In Section 3, the attenuation of X-ray signals in Mars entry blackout is estimated. Moreover, the positioning performance is evaluated and the influence of X-ray signal transmission system on the positioning error is analyzed. Finally, Section 4 contains the conclusion and future research directions.

2. Theories and methods

2.1. X-ray-based positioning method

The strategy using radio beacons to transmit RF signals for the position estimation of Mars entry vehicles has been studied in preceding research. X-ray signals can be utilized to reach the same goal. Part of the signal processing of X-rays is similar to RF signals. The main difference is that the emission and detection of X-ray signals are realized by a modulated X-ray source (transmitter) and an X-ray detector module (receiver), respectively. Furthermore, in the traditional scheme using RF signals, as the technology of RF signals receiving and processing is

* Corresponding author.
E-mail address: tangxiaobin@nuaa.edu.cn (X. Tang).

https://doi.org/10.1016/j.apradiso.2020.109518
Received 17 July 2020; Received in revised form 8 October 2020; Accepted 12 November 2020
Available online 18 November 2020
0969-8043/© 2020 Elsevier Ltd. All rights reserved.

relatively mature, each radio beacon just needs to transmit signals and the entry vehicle only receives and processes the signal. However, X-ray detectors cannot identify several simultaneously arrived signals due to the restriction of current technologies. Therefore, the entry vehicle carries modulated X-ray sources and an X-ray detector in this design. The modulated X-ray sources emit the positioning signal to orbiters through the collimation design in different directions. Each orbiter also carries an X-ray detector to receive the signal. Besides, the orbiter which equipped with the data processing center carries a modulated X-ray source to emit X-ray signals. There also has an acquisition pointing and tracking system which maintains the link alignment. The development of above-mentioned technologies and devices has been conducted in a number of XCOM research work, and XCOM experimental test has also been carried out on International Space Station in 2019 (Lori, 2019; Timofeev et al., 2019). Thus, it is available to establish the X-ray positioning signal transmission link between the entry vehicle and orbiters during Mars entry blackout.

The schematic diagram of the proposed method is illustrated in Fig. 1. It is assumed that several orbiters are put into place in advance, which is consistent with the traditional radio beacon based scheme. This method is realized through a six-step process. First, the entry vehicle switches on the X-ray signal transmitter when it reaches the altitude of Mars entry blackout and the time information is transmitted to each orbiter as an X-ray signal. Second, the receiver carried by each orbiter receives the X-ray signal and records the time of signal arrival, and the time of signal emission is obtained by demodulating the received signal. Then the pseudorange between each orbiter and the entry vehicle is calculated by the time difference between the time of signal emission and arrival. The pseudorange represents that the range value is not a true geometric distance between the entry vehicle and orbiters. Next, each orbiter transmits the pseudorange information to the data processing center. Note that the pseudorange information can be transmitted through RF signals between orbiters and the data processing center. The main reason is that the Martian atmosphere is so thin at the altitude of orbiters that Mars entry blackout will not occur, and the RF signal transmission technology is relatively mature. Afterwards, the position coordinates of the entry vehicle can be obtained by the data processing center through the calculation of the received pseudorange information and known orbital parameters. The data processing center also sends the coordinates to the entry vehicle using X-ray signals. In the end, the entry vehicle demodulates the signal containing its position coordinates and thus determines its location.

2.2. Theory of X-ray signal transmission

Predicting the signal attenuation is of great importance for illustrating the superiority of X-rays. The attenuation of X-ray signals during Mars entry blackout are mainly caused by the plasma sheath and Martian atmosphere. The Wentzel–Kramer–Brillouin method (Appendix A) was used to analyse the interaction between X-ray signals and plasma sheath. The electron density of the plasma sheath is a critical parameter that determines the signal attenuation. Fig. 2(a) presents the electron density distribution of the plasma sheath. The stagnation point and the wake region are two areas where the electron density of the entry vehicle surface reaches the maximum and minimum, respectively. The Monte Carlo simulation method was employed to calculate the transmission coefficient of X-ray signals in Martian atmosphere. The interaction between X-rays and Martian atmosphere has been conducted in our preceding work of XCOM (Hang et al., 2019). The previously used atmospheric model was a simplified model which was layered vertically. However, the Martian atmosphere is spherical around the Mars surface. Therefore, a spherical layered model was used in this analysis. The Martian atmosphere was modeled at one layer per kilometre because the atmospheric density varies with the altitude, as shown in Fig. 2(b). The orbiter altitude was fixed at 150 km (Zurek et al., 2015). The entry vehicle altitude was set with a range of 20 km–100 km. The Mars entry blackout occurred in this altitude range according to the data of Mars Science Laboratory (MSL) (Karlgaard et al., 2013). Due to the high-speed flight of the entry vehicle and each orbiter, changes about link elevation angle were also considered. The atmospheric density was estimated by the traditional exponential model (Mazarico et al., 2007).

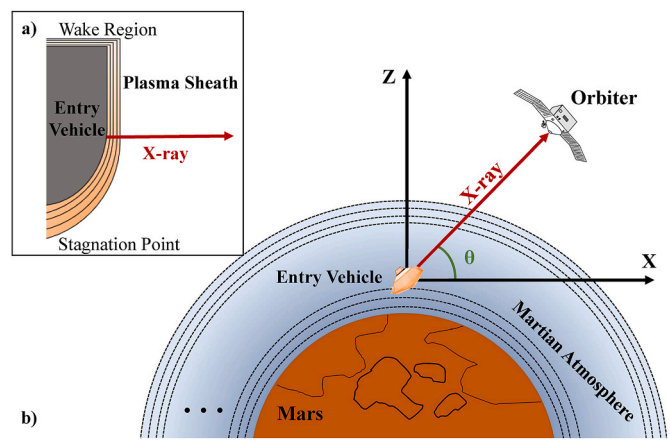

Fig. 2. The model for signal attenuation analysis of X-rays in the (a) plasma sheath and (b) Martian atmosphere.

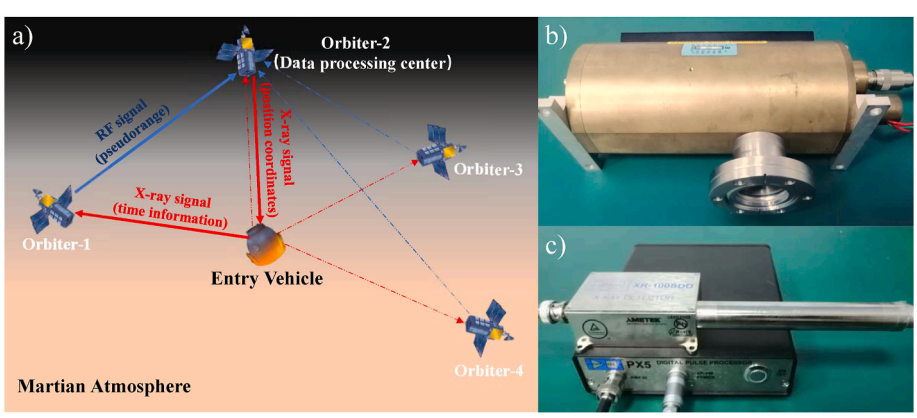

Fig. 1. (a) Schematic diagram of the X-ray-based positioning method; the (b) modulated X-ray source and (c) X-ray detector module that can be used in X-ray signal transmission system.

2.3. Measurement model

The position of the entry vehicle can be estimated by the measurement model. There are four X-ray signal transmission links since that four unknown parameters (the three-dimensional coordinates and the clock offset) are considered here. As shown in Fig. 3, one link is used as examples for description. T_s is the system time when the positioning signal leaves the entry vehicle. T_o is the system time when the signal reaches the orbiter. Due to the clock frequency on entry vehicle is difficult to keep same with the ones on orbiters, which easily leads to the clock offset in the time benchmark of the entry vehicle and orbiters. t is the offset between the entry vehicle's clock and system time. δ_t is the offset between the orbiter's clock and system time. The time obtained by the orbiter's clock can be written as $T_s + \delta_t$, and the time received by the entry vehicle's clock can be presented as $T_o + t$. Several measurement biases (ε_p) may be caused by the link clutter, such as the ionospheric delay and the tropospheric delay. Therefore, the actual geometric distance (r) and the pseudorange (ρ) can be reconstructed as

$$r = c(T_o - T_s), \tag{1}$$

$$\rho = c\left[T_o + t - (T_s + \delta_t) + \varepsilon_p\right] = r + c\left(t - \delta_t + \varepsilon_p\right), \tag{2}$$

where δ_t can be corrected by monitoring the orbiter and can be regarded as known. ε_p was treated as a Gaussian-distribution:$\varepsilon_p \tilde{} N(10, 1)$, whose unit is the meter (Martin, 1978). The simplified assumption can be accepted since that the transmission of X-rays is weakly influenced by the scattering and refraction of the Martian atmosphere.

The pseudorange obtained from the X-ray detector module is transmitted to the data processing center for position coordinates calculation. The coordinates of each orbiter and the entry vehicle are unified to Mars fixed coordinate system. The position coordinates of the entry vehicle are defined by (x, y, z), and the known position coordinates of Orbiter-i are given by (x_i, y_i, z_i). r_i and ρ_i can be modeled by

$$r_i = \sqrt{(x_i - x)^2 + (y_i - y)^2 + (z_i - z)^2}, \tag{3}$$

$$\rho_i = f(x, y, z, t) = r_i + c\left(t - \delta_t + \varepsilon_p\right), \tag{4}$$

where i is the serial number of each orbiter. If the approximate position coordinates of the entry vehicle are known as (x', y', z') and the corresponding clock offset is t', then the pseudorange between the approximate and real position can be written as

$$\rho_i' = f(x', y', z', t'), \tag{5}$$

$$\rho_i = f(x' + \Delta x, y' + \Delta y, z' + \Delta z, t' + \Delta t), \tag{6}$$

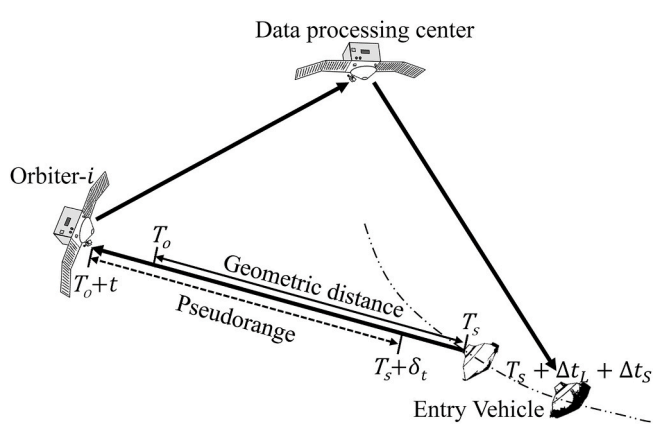

Fig. 3. The measurement model of the X-ray positioning signal transmission link.

where Δx, Δy, and Δz means the deviation between the approximate position and real position at time T_s. Expanding and ignoring the term after the first-order partial derivative. The four signal transmission links satisfy the following formula

$$\Delta\rho = H\Delta X, \tag{7}$$

where

$$\Delta\rho = \begin{bmatrix} \Delta\rho_1 \\ \Delta\rho_2 \\ \Delta\rho_3 \\ \Delta\rho_4 \end{bmatrix}, H = \begin{bmatrix} a_{x1} & a_{y1} & a_{z1} & 1 \\ a_{x2} & a_{y2} & a_{z2} & 1 \\ a_{x3} & a_{y3} & a_{z3} & 1 \\ a_{x4} & a_{y4} & a_{z4} & 1 \end{bmatrix}, \Delta X = \begin{bmatrix} \Delta x \\ \Delta y \\ \Delta z - c\Delta t \end{bmatrix}.$$

where a_{xi}, a_{yi}, and a_{zi} represent the direction cosine of the unit vector pointing from the approximate position to Orbiter-i. Therefore, the coordinates of the estimated position at time T_s can be derived from the deviation (ΔX) and the approximate position coordinates. Besides, a more accurate solution can be obtained by iterating the above process.

When the entry vehicle emits an X-ray positioning signal at time T_s, the time when the estimated position coordinates are received can be indicated as $T_s + \Delta t_L + \Delta t_S$ due to the high-speed flight of the entry vehicle. The Δt_L and Δt_S denote the link transmission delay and the signal emission delay caused by the modulation rate of X-ray sources, respectively. Therefore, the pseudorange measurement bias is just one of the positioning error sources, and the time delay from emitting the X-ray positioning signal to receiving position coordinates is also a significant error source. When the position coordinates received can be expressed by $(x_{T_s}, y_{T_s}, z_{T_s})$, whose calculation has taken into account the pseudorange measurement bias, the actual coordinates of the entry vehicle can be given as $(x_{T_s+\Delta t_L+\Delta t_S}, y_{T_s+\Delta t_L+\Delta t_S}, z_{T_s+\Delta t_L+\Delta t_S})$. Thus, the positioning error can be determined by

$$\varepsilon = \sqrt{P^T P}, \tag{8}$$

where

$$P = \begin{bmatrix} x_{T_s+\Delta t_L+\Delta t_S} - x_{T_s} \\ y_{T_s+\Delta t_L+\Delta t_S} - y_{T_s} \\ z_{T_s+\Delta t_L+\Delta t_S} - z_{T_s} \end{bmatrix}.$$

Additionally, the time delay can be obtained by

$$\Delta t_L = L/V, \tag{9}$$

$$\Delta t_S = I/R, \tag{10}$$

where L is the link distance; V is the propagation velocity, which was approximated as the speed of light; I is the amount of information transmitted in the positioning signal, which was estimated at 100 bits according to the time stamp and position coordinates; and R is the data rate. The other delays are caused by the emission and reception of RF signals, which are negligible because the data rate of RF signal transmission has exceeded several megabits per second (Haskins and Millard, 2010).

2.4. X-ray signal transmission link model

The above analyses have shown that the time delay is an important error source. Therefore, data rate is an important parameter that limits the positioning performance. The signal transmitting power also affects the data rate. The link model was built to evaluate the influence of the X-ray signal transmitting power. The CdZnTe detector was employed as the detection module (Kim et al., 2020). The 4-level pulse-position-modulation method was adopted. The bit-error-rate, signal-to-noise ratio, and signal transmitting power of one signal transmission link can be obtained by (Zhou et al., 2019)

$$BER = 0.5 \times \mathrm{erfc}\left(\sqrt{SNR} \Big/ 2\sqrt{2}\right), \tag{11}$$

$$SNR = \left((\eta_d q P_r / h\nu)^2 \Big/ 2q^2(\eta_d F_u A_r + (P_r \eta_d / h\nu) + I_d / q) + 4KT \Big/ R_l \right) \Big/ R, \tag{12}$$

$$P_r = P_t \times \eta_{pla} \times \eta_{atm} \times A_r \Big/ \pi(\tan(0.5\omega)L)^2, \tag{13}$$

where P_r is the signal receiving power; R_l is the equivalent impedance; the detection efficiency (η_d) was more than 90%; and the collection area (A_r) was 1 m^2 (Quadrini et al., 2005). The flux of background X-rays (F_u) was 50 $m^{-2}{\cdot}s^{-1}$ (Wei et al., 2013). The divergence angle (ω) was 0.5mrad (Liu et al., 2016). The transmission coefficients of the plasma sheath (η_{pla}) and Martian atmosphere (η_{atm}) were determined with the calculation of X-ray signal attenuation. As several positioning signal transmission links are needed to determine position coordinates, the signal transmitting power of the system can be expressed as

$$P = \sum_{j=1}^{i} P_t^j. \tag{14}$$

3. Results and analysis

3.1. X-ray signal attenuation

The X-ray signal presents high penetration during Mars entry blackout. The trend of transmission and attenuation coefficients as a function of carrier frequency is shown in Fig. 4. The signal attenuation is considerably affected by the plasma sheath of Mars entry blackout in the RF range. In the stagnation point ($n_{emax} = 9.0 \times 10^{18}$ m^{-3}) of the entry vehicle surface, the maximum attenuation coefficient is over 300 dB for the UHF-band (400 MHz) or X-band (8.4 GHz) signal that is commonly used in Mars missions, which is almost impossible to penetrate the plasma sheath. In the wake region ($n_{emax} = 8.4 \times 10^{16}$ m^{-3}), although the attenuation coefficient is reduced, the maximum still reaches about 30 dB. However, X-ray (10^{17}–10^{19} Hz) signals belong to the high frequency range. Its attenuation coefficient is close to zero after penetrating the same plasma sheath. Therefore, the disruption of the plasma sheath to the positioning signal transmission can be avoided by using X-rays.

The transmission properties of 10 keV and 70 keV X-ray signals in the Martian atmosphere are shown in Fig. 5. The results indicate that X-rays with an energy range of 10 keV–70 keV can be utilized to achieve the uninterrupted signal transmission for different altitudes during Mars entry blackout. At the beginning of the Mars entry blackout, the transmission coefficient of 10 keV X-ray signals exceeds 0.9, and the 10 keV X-rays can be used to establish a stable link in this case. However, with the decrease of the entry vehicle's altitude, especially about 25 km from Martian surface, the entry vehicle is still at the end of Mars entry blackout. The 10 keV X-ray signal is completely unable to penetrate the Martian atmosphere at this time, while the transmission coefficient of the 70 keV X-ray still exceeds 0.5. In addition, maintaining a large elevation angle is conducive to improve the positioning signal transmission link stability because the transmission coefficient increases with the elevation angle.

3.2. Positioning performance

The scenario of Mars entry blackout was simulated to assess the positioning performance, as shown in Fig. 6. The simulation began at 22:25:00 UTC on Aug 5, 2012 and lasted about 60 s (Israel et al., 2016; Morabito and Edquist, 2005). The simulation sample step was set to 1 s. Due to the X-ray signal transmission coefficient is higher at large elevation angles, and the positioning accuracy increases with the geometric distribution uniformity of orbiters improve, the orbital parameters are designed with the two factors and presented in the table of Fig. 6. The system visibility can be maintained through the design. The movement of the entry vehicle was reconstructed with reference to MSL (Karlgaard et al., 2013), whose changes in the trajectory and velocity are shown in Fig. 6. Fig. 7 indicates the statistical results of the link distance and elevation angle. It should be noted that the link distance includes the X-ray and RF signals transmission links. Moreover, the link distance and elevation angle change over time because of the high-speed flight of each orbiter and the entry vehicle. The upward or downward trend of the curve depends on the relative position between each orbiter and the entry vehicle. In addition, to estimate the position coordinates, the pseudorange was deduced from the signal transmission time delay, which is determined by the link geometric distance as well as by the clock offset and the link clutter. From the simulation model, the geometric distance between the entry vehicle and each orbiter at any sample step can be got through obtaining the coordinates of the entry vehicle and orbiters at any time, as shown in Fig. 7. Moreover, the clock offset of 300 ns was used in the simulation, which is the maximum in the current navigation satellite. We also estimate the time delay caused by the link clutter according to Eq. (2).

The data rate was set to 50 kbps which has been achieved in XCOM, and the bit-error-rate was set to 10^{-6} to estimate the positioning error (Israel et al., 2016). The energy of the X-ray positioning signal was set to 70 keV to ensure the X-ray positioning signal transmission link stability (Fig. 5). The results are shown in Fig. 8. In the whole simulation process, the maximum positioning error is about 68 m, the minimum is about 27 m, and the mean value is about 43.2 m. Furthermore, there is a trend that the positioning error decreases with the time of the entry vehicle entering the blackout increase. This is because that the entry vehicle speed decreases gradually during Mars entry blackout (Fig. 6(b)). Therefore, at the same time interval, the entry vehicle displacement in the latter part of Mars entry blackout is less than that in the previous part, resulting in the decrease in positioning error. This indicates that the X-ray-based positioning method is expected to obtain a better positioning accuracy compared with traditional IMU whose positioning

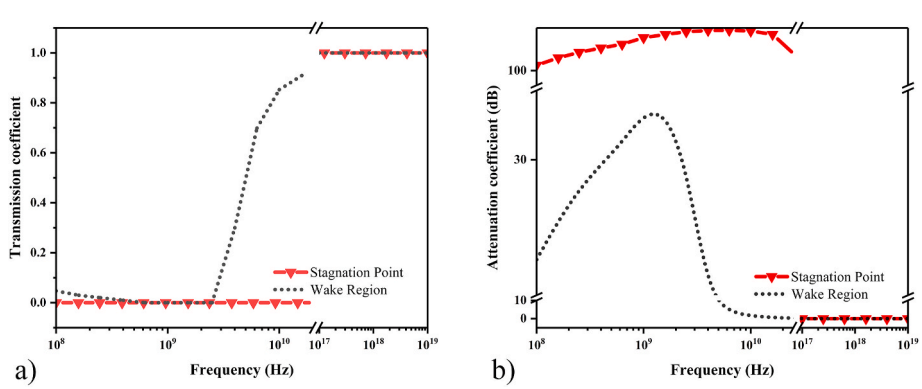

Fig. 4. (a) Transmission coefficient and (b) attenuation coefficient of X-ray signals in the plasma sheath during Mars entry blackout.

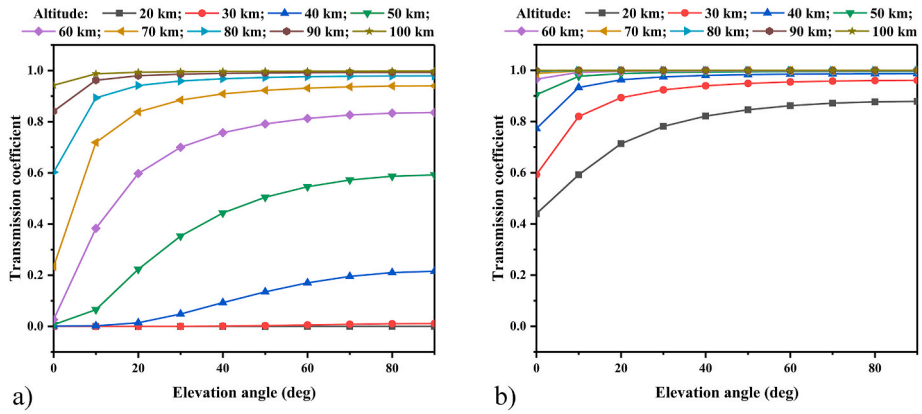

Fig. 5. X-ray transmission coefficient at different energy levels of (a) 10 keV and (b) 70 keV in Martian atmosphere.

a)

Table. Parameters of orbital design.

Parameters	Orbiter-1	Orbiter-2	Orbiter-3	Orbiter-4
Semi-major Axis (km)	3546.19	3546.19	3546.19	3546.19
Eccentricity	0	0	0	0
Inclination (deg)	6	175	60	60
Argument of Perigee (deg)	0	0	0	0
RAAN (deg)	100	270	-35	140

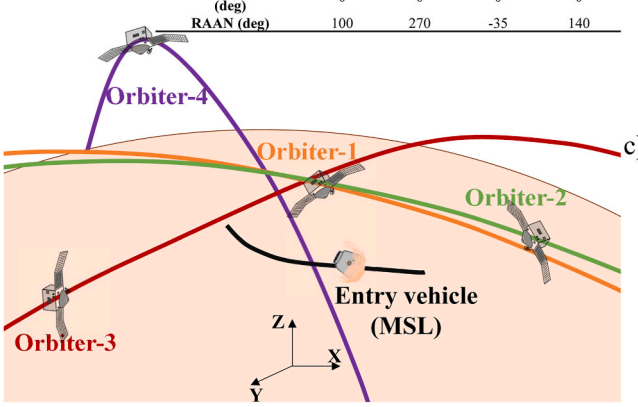

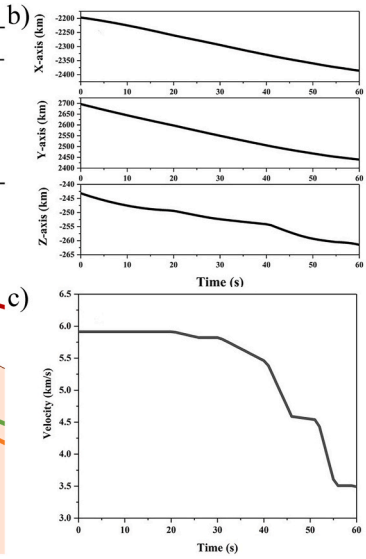

Fig. 6. (a) Simulation scenario created for the positioning performance analysis; (b) Trajectory coordinates and (c) velocity of the entry vehicle.

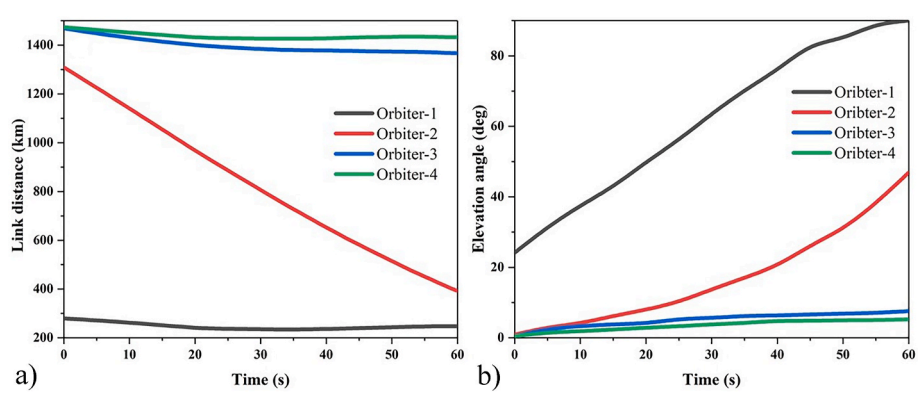

Fig. 7. (a) Link distance and (b) elevation angle of the signal transmission link between the entry vehicle and each orbiter.

error exceeds a few hundred meters.

3.3. Influence of X-ray signal transmission system

The data rate is a critical parameter that limits the signal emission delay. Therefore, analyzing the effect of data rate is beneficial to provide a theoretical basis for the X-ray signal transmission system design. The trend of the positioning error with different data rates is shown in Fig. 9. The positioning error can be considerably reduced by increasing the data rate within a certain range. When the data rate of X-ray positioning signals increases from 10 kbps to 128 kbps, the mean positioning error decreases from 113 m to 37 m. In addition, the maximum and minimum positioning errors also decrease as the data rate increase. This is because that increasing the data rate is conducive to reduce the signal emission

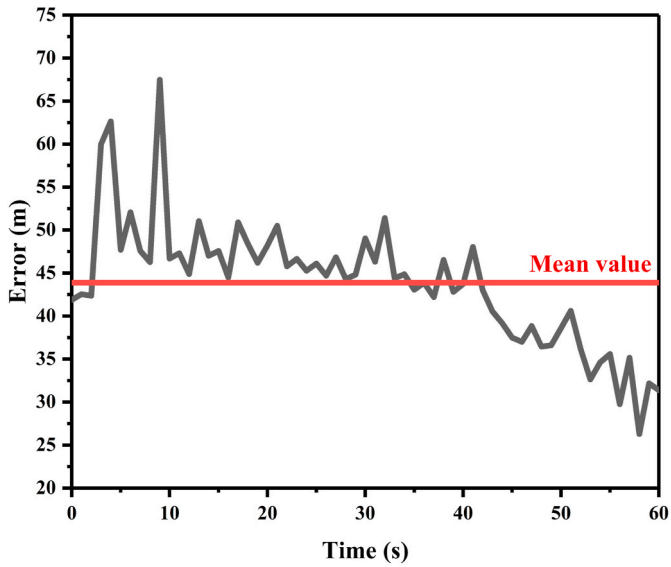

Fig. 8. The positioning error of the X-ray-based positioning method during Mars entry blackout.

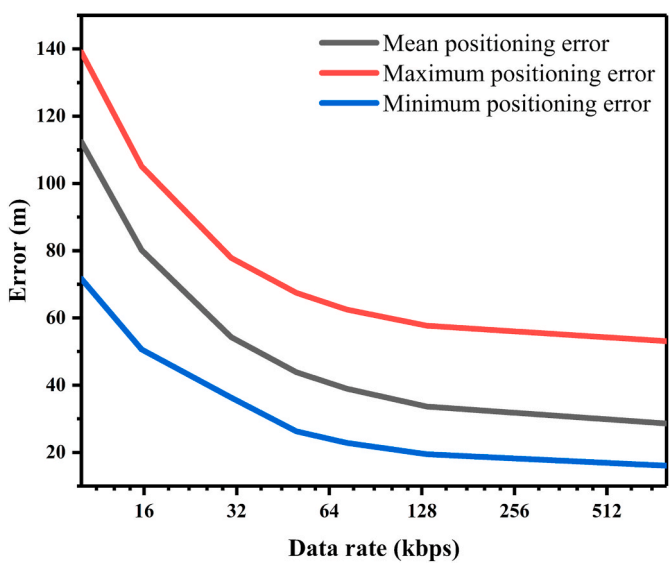

Fig. 9. The relationship of the positioning error with different data rates.

delay (Eq. (10)). However, the influence of data rate on the positioning error is limited in a higher range since that the data rate is so high that the signal emission delay can be neglected. When data rate increases from 128 kbps to 800 kbps, the positioning error reduction is less than 10 m.

The signal transmitting power also affects the data rate in the X-ray signal transmission system. To obtain the satisfactory positioning accuracy and data rate, the influence of signal transmitting power is also discussed here. The relationship of the mean positioning error and data rate with different levels of signal transmitting power is shown in Fig. 10. The results demonstrate that improving the signal transmitting power within a certain range is an effective means for reducing the positioning error. When the signal transmitting power increases from 21 W to 66 W, the data rate increases from 10 kbps to 128 kbps, and the corresponding mean positioning error decreases from 113 m to 37 m. This is because that increasing the signal transmitting power is beneficial to increase the data rate in the X-ray signal transmission system (Fig. 10). However, the signal transmitting power available to the

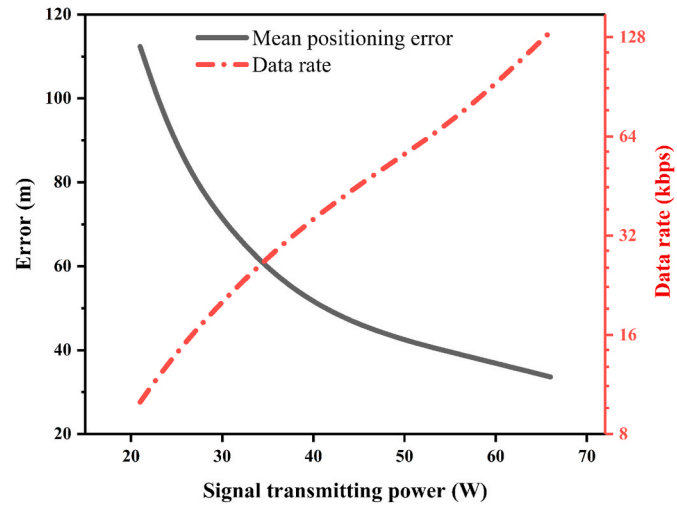

Fig. 10. The mean positioning error and data rate with different levels of signal transmitting power.

system is usually restricted due to the power distribution limitation. Thus, the determination of the data rate requires a comprehensive consideration of the influence of positioning error and signal transmitting power. The data rate that can be achieved in XCOM has exceeded 50 kbps, and the corresponding signal transmitting power of this data rate with the four links is about 47 W. It should be noted that the signal transmitting power is not exactly equal to the power needed. The needed power is also related to the technical scheme of the X-ray signal emission source adopted. The electricity demand can be satisfied since that the power source can provide electric power of more than 350 W during Mars entry phase (Ciancetta et al., 2017).

4. Conclusion

This study developed an X-ray-based positioning method for addressing the difficulty of limited access to positional information during Mars entry blackout. This scheme was preliminary analyzed with the simulation method. The results demonstrated that X-rays can be utilized to establish a stable positioning signal transmission link because that the X-ray signal attenuation in the plasma sheath and Martian atmosphere is extremely low. Additionally, this method could maintain a relatively low positioning error. The maximum positioning error of about 68 m, minimum of about 27 m and mean value of about 43.2 m could be achieved if the X-ray signal transmission link with the energy of 70 keV, data rate of 50 kbps, BER of 10^{-6} and signal transmitting power of 47 W. Moreover, the positioning error could be effectively reduced by improving the data rate and signal transmitting power within a certain range where the data rate and signal transmitting power do not exceed 128 kbps and 66 W, respectively. These results indicate that the X-ray-based positioning method would be a potential application for enhancing the positional information acquisition during Mars entry blackout in future Mars landing missions.

Although this scheme presents advantages in the mitigation of Mars entry blackout, there still have some aspects that could be strengthened. It may be possible to reduce the number of orbiters, power consumption and obtain more state information if this design can be integrated with other strategies such as IMU and the CubeSat technology. Moreover, the quantitative analysis of the pseudorange measurement errors caused by the effect of the Martian atmosphere on X-ray signal transmission is still needed to study. These issues must be performed in the future research.

CRediT authorship contribution statement

Peng Dang: Methodology, Data curation, Writing - original draft,

Visualization. **Xiaobin Tang:** Conceptualization, Supervision, Writing - review & editing. **Yunpeng Liu:** Validation, Software, Resources. **Junxu Mu:** Data curation, Software. **Sheng Lai:** Software.

Declaration of competing interest

The authors declare that they have no known competing financial interests or personal relationships that could have appeared to influence the work reported in this paper.

Acknowledgements

This work was supported by the Aeronautical Science Fund (Grant No. 2018ZC52029), and the State Key Laboratory of Simulation and Effects of Intense Pulse Radiation Environment [Grant No. SKLIPR1813].

Appendix A. The Wentzel–Kramer–Brillouin method for signal attenuation calculation in the plasma sheath

The electron density distribution of the entry vehicle surface usually can be approximated as

$$n_e(z) = \begin{cases} n_{emax} exp\left(a_1(z-z_0)^2\right) & (0 \le z \le z_0) \\ n_{emax} exp\left(-a_2(z-z_0)^2\right) & (z_0 \le z \le z_1) \end{cases}, \tag{A.1}$$

where n_{emax} represents the peak electron density, which was set with reference to MSL. Additionally, $a_1 = 0.5$, $a_2 = 1$, $z_0 = 0.05$ m and $z_1 = 0.15$ m are parameters to describe the electron density distribution. z is the propagation length. The plasma frequency can be expressed as

$$\omega_P = \sqrt{n_e(z)e^2/m_e\varepsilon_0} \tag{A.2}$$

The relative dielectric constant can be written as

$$\varepsilon_r = 1 - \omega_p{}^2 / \left(\omega^2 + \nu^2\right) - j(\nu/\omega)\left(\omega_p{}^2 / \left(\omega^2 + \nu^2\right)\right), \tag{A.3}$$

where $\nu = 1 \times 10^9$ Hz is the collision frequency; ω is the angular frequency. The propagation constant is given as

$$k = (\omega/c)\sqrt{\varepsilon_r} = k_r + jk_i, \tag{A.4}$$

where k_r and k_i are the real and imaginary parts of the propagation constant, respectively. The transmission coefficient (T) and attenuation coefficient (Att) satisfy

$$T = \exp(-2k_i z), \tag{A.5}$$

$$Att = 8.686|k_i|z. \tag{A.6}$$

References

Ciancetta, E., Cuzzocrea, G., Digoin, J.-J., et al., 2017. Exomars 2016 Mission Electrical Power System. E3S Web of Conferences, vol. 16, p. 13012. https://doi.org/10.1051/e3sconf/20171613012. Fernandez, A, EDP SCIENCES, CEDEX A.

Drake, B.G., Hoffman, S.J., Beaty, D.W., 2010. Human exploration of Mars, design reference architecture 5.0. In: IEEE Aerospace Conference, pp. 1–24. https://doi.org/10.1109/AERO.2010.5446736.

Economou, T.E., 2010. Application of radioactive sources in analytical instruments for planetary exploration. Appl. Radiat. Isot. 68, 542–545. https://doi.org/10.1016/j.apradiso.2009.09.011.

Hang, S., Tang, X., Li, H., et al., 2019. Novel approach for Mars entry blackout elimination based on X-ray communication. J. Spacecr. Rockets 56, 1546–1552. https://doi.org/10.2514/1.A34421.

Haskins, C.B., Millard, W.P., 2010. Multi-band software defined radio for spaceborne communications, navigation, radio science, and sensors. IEEE Aerospace Conference 1–9. https://doi.org/10.1109/AERO.2010.5446908.

Hastrup, R., Bell, D., Cesarone, R., et al., 2003. Mars network for enabling low-cost missions. Acta Astronaut. 52, 227–235. https://doi.org/10.1016/S0094-5765(02)00161-3.

Israel, D.J., Heckler, G.W., Menrad, R.J., 2016. Space mobile network: a near earth communications and navigation architecture. IEEE Aerospace Conference 1–7. https://doi.org/10.1109/AERO.2016.7500669.

Jah, M.K., Lisano, M.E., Born, G.H., et al., 2008. Mars aerobraking spacecraft state estimation by processing inertial measurement unit data. J. Guid. Control Dyn. 31, 1802–1812. https://doi.org/10.2514/1.24304, 2008.

Karlgaard, C.D., Kutty, P., Schoenenberger, M., Shidner, J., 2013. Mars Science Laboratory entry, descent, and landing trajectory and atmosphere reconstruction. Adv. Astronaut. Sci. 148, 1555–1574.

Lori, Keesey, 2019. NASA Set to Demonstrate X-Ray Communications in Space. Web Document. URL: https://phys.org/news/2019-02-nasa-x-ray-space.html.

Kim, M., Gülhan, A., 2011. Plasma Manipulation Using a MHD-Based Device for a Communication Blackout in Hypersonic Flights. IEEE, Piscataway, pp. 412–417. https://doi.org/10.1109/RAST.2011.5966868. Proceedings of the 2011 5th International Conference on Recent Advances in Space Technologies (RAST).

Kim, B.J., Lee, K.B., Lee, J.M., et al., 2020. Design of optimal digital filter and digital signal processing for a CdZnTe high resolution gamma-ray system. Appl. Radiat. Isot. 162, 109171. https://doi.org/10.1016/j.apradiso.2020.109171.

Lévesque, J.F., De Lafontaine, J., 2007. Innovative navigation schemes for state and parameter estimation during Mars entry. J. Guid. Control Dyn. 30, 169–184. https://doi.org/10.2514/1.25107.

Li, S., Jiang, X., 2014. Review and prospect of guidance and control for Mars atmospheric entry. Prog. Aeosp. Sci. 69, 40–57. https://doi.org/10.1016/j.paerosci.2014.04.001.

Li, S., Peng, Y., 2011. Radio beacons/IMU integrated navigation for Mars entry. Adv. Space Res. 47, 1265–1279. https://doi.org/10.1016/j.asr.2011.01.001.

Li, H., Tang, X., Hang, S., Liu, Y., et al., 2017. Potential application of X-ray communication through a plasma sheath encountered during spacecraft reentry into earth's atmosphere. J. Appl. Phys. 121, 123101. https://doi.org/10.1063/1.4978758.

Li, Y., Su, T., Sheng, L., et al., 2020. Simulation and experiment of X-ray communication in re-entry dusty plasma region. Mod. Phys. Lett. B 34, 2050057. https://doi.org/10.1142/S0217984920500578.

Lightsey, E.G., Mogensen, A.E., Burkhart, P.D., Ely, T.A., Duncan, C., 2008. Real-time navigation for Mars missions using the Mars network. J. Spacecr. Rockets 45, 519–533. https://doi.org/10.2514/1.30974.

Liu, D., Qiang, P.-F., Li, L.-S., et al., 2016. X-ray focusing optics and its application in X-ray communication system. Acta Phys. Sin. 65, 010703 https://doi.org/10.7498/aps.65.010703.

Martin, E.H.J.N., 1978. GPS user equipment error models. Navigation 25, 201–210. https://doi.org/10.1002/j.2161-4296.1978.tb01331.x.

Mazarico, E., Zuber, M.T., Lemoine, F.G., Smith, D.E., 2007. Atmospheric density during the aerobraking of Mars Odyssey from radio tracking data. J. Spacecr. Rockets 44, 1165–1171. https://doi.org/10.2514/1.28448.

Morabito, D.D., Edquist, K.T., 2005. Communications blackout predictions for atmospheric entry of Mars Science Laboratory. IEEE Aerospace Conference, pp. 489–500. https://doi.org/10.1109/AERO.2005.1559339.

Quadrini, E.M., Conti, G., D'Angelo, S., et al., 2005. CZT Detectors for a New Generation of γ-ray Telescopes. Proc. SPIE 5898, UV, X-Ray, and Gamma-Ray Space Instrumentation for Astronomy XIV, 58980O. https://doi.org/10.1117/12.616686.

Ramjatan, S., Magin, T., Scholz, T., Van der Haegen, V., Thoemel, J., 2017. Blackout analysis of small cone-shaped reentry vehicles. J. Thermophys. Heat Tran. 31, 269–282. https://doi.org/10.2514/1.T4825.

Salotti, J.-M., Heidmann, R., 2014. Roadmap to a human Mars mission. Acta Astronaut. 104, 558–564. https://doi.org/10.1016/j.actaastro.2014.06.038.

Timofeev, G., Potrakhov, N., Nechaev, A., 2019. Experimental Research of the X-Ray Communication System. AIP Conference Proceedings. 2089. AIP Publishing LLC, 020020. https://doi.org/10.1063/1.5095749.

Wang, X., Xia, Y., 2015. Navigation strategy with the spacecraft communications blackout for Mars entry. Adv. Space Res. 55, 1264–1277. https://doi.org/10.1016/j.asr.2014.11.021.

Wei, E., Jin, S., Zhang, Q., Liu, J., Li, X., Yan, W., 2013. Autonomous navigation of Mars probe using X-ray pulsars: modeling and results. Adv. Space Res. 51, 849–857. https://doi.org/10.1016/j.asr.2012.10.009.

Yu, Z., Cui, P., Crassidis, J.L., 2017. Design and optimization of navigation and guidance techniques for Mars pinpoint landing: review and prospect. Prog. Aeosp. Sci. 94, 82–94. https://doi.org/10.1016/j.paerosci.2017.08.002.

Zhou, W., Tang, X., Liu, Y., et al., 2019. Power budget and performance analysis of X-ray communication during the Earth re-entry of spacecraft. Optik 199, 163521. https://doi.org/10.1016/j.ijleo.2019.163521.

Zurek, R.W., Tolson, R.H., Baird, D., Johnson, M.Z., Bougher, S.W., 2015. Application of MAVEN accelerometer and attitude control data to Mars atmospheric characterization. Space Sci. Rev. 195, 303–317. https://doi.org/10.1007/s11214-014-0095-x.